Crystal Growth

International Edition: DOI: 10.1002/anie.201510376
German Edition: DOI: 10.1002/ange.201510376

Inverted Wedding Cake Growth Operated by the Ehrlich–Schwoebel Barrier in Two-Dimensional Nanocrystal Evolution

*Xin Yin, Dalong Geng, and Xudong Wang**

Abstract: *Wedding cake growth is a layer-by-layer growth model commonly observed in epitaxial growth of metal films, featured by repeated nucleation of new atomic layers on the topmost surface owing to the confinement of the Ehrlich–Schwoebel (ES) barrier. Herein, we report an inverted wedding cake growth phenomenon observed in two-dimensional nanostructure evolution. Through a dynamically controlled vapor–solid deposition process of ZnO, a unique basin-shaped crown was formed on the tip of each nanowire, featured with concentric steps. The atomic steps were nucleated along the edge and propagated toward the center. This is an opposite growth behavior compared to the conventional wedding cake growth, and is thus denoted as inverted wedding cake growth. Through the relation between the crown expansion rate and the temperature, the ES barrier of ZnO was determined to be 0.88 eV. The discovery of inverted wedding cake growth provided insight into the developing nanostructure growth mechanisms.*

Precisely controlling dimension and morphology are critical elements enabling enhanced and tunable physical and/or chemical properties with promising application potentials in electronics, photonics, energy, and biology.[1] For example, zero dimensional quantum dots are featured by their tunable band gaps and discrete density of states owing to the size-dependent quantum confinement effect, yielding tremendous application potential in biomedical devices, quantum computing, light emitting devices, photodetectors, and solar energy harvesters.[2] One-dimensional (1D) nanowire (NW) or nanotube structures could act as confined channels for transporting and manipulating electrons, photons, and phonons.[3] Two-dimensional (2D) sheet morphology offers both quantum-confined physical properties and fabrication/processing friendliness, quickly leading them to be a new focus in the large family of nanomaterial systems.[4] Although these morphologies are strikingly different in their geometry, they may share certain basic crystal growth mechanisms. Subtle variations in local kinetics would be largely magnified during the crystal growth, leading to distinguishing final structures. Therefore, for scalable nanomanufacturing, an indispensable prerequisite is to understand the atomistic mechanisms and advanced kinetics that govern the morphology evolution at the nanoscale.

Among the splendid nanoscale structures, the NW morphology has long been used as a model system to explore anisotropic crystal growth behavior. Metal catalyst was typically introduced to direct NW growth, and the vapor–liquid–solid (VLS) process was the most widely accepted growth mechanism.[5] Additionally, the vapor–solid–solid (VSS) process became more commonly seen for the cases where the catalyst could not reach the liquid state. Through real-time observations, a ledge flow mechanism, including step nucleation and flow, has been proposed for VSS growth of NWs in the presence of catalysts.[6] When there is no catalyst present, crystal growth typically follows the vapor–solid (VS) process.[7] The oriented attachment through preferred stacking of nanocrystals along their high energy surfaces and the screw dislocation-driven growth are two representative growth mechanisms governing VS NW growth.[8] Most recently, by dynamically controlling the deposition conditions, our group captured a unique concentric terrace feature on the top surface of nanoplates and NWs, which led to the discovery of the wedding cake growth model.[5c] In this paper, a series of single crystal hexagonal branch-crowned ZnO NW structures were obtained by dynamically changing the deposition temperature during the growth. The top structure was found to be a basin-like concave crown with six equivalent extended branches. An inverted wedding cake growth model involving the Ehrlich–Schwoebel (ES) barrier and step propagation along the top surface edge was developed to explain the growth mechanism. By changing the oxygen partial pressure and deposition temperature, the ES barrier of ZnO was quantified. This research further enriches our understanding of nanoscale crystal growth kinetics and suggests that the layer-by-layer growth model could be one major crystal growth mechanism in forming nanostructures from the bottom up.

Dynamically controlled VS growth of ZnO nanostructures was carried out under dynamically-tuning deposition conditions (Supporting Information, Methods). Both the evaporation and deposition temperature was increased during growth, providing a non-steady state growth environment that yielded a unique morphology-switch growth phenomenon, where all the NWs were capped with a significantly broadened crown, as shown by the side-viewed SEM image in Figure 1 a. In contrast to our previous observations of the hexagon-capped nanopillars,[5c] all of the top crowns exhibited clear six-fold branches with uniform sizes and distributions (Figure 1 b). Figure 1 c shows a typical structure of the hybrid morphology. The NW had a diameter of 500 nm and a length of 30 μm. The crown had a core diameter of 3 μm

[*] X. Yin, D. L. Geng, Prof. X. D. Wang
Department of Material Sciences and Engineering
University of Wisconsin-Madison
1500 Engineering Dr., Madison, WI 53705 (USA)
E-mail: xudong@engr.wisc.edu

Supporting information for this article is available on the WWW under http://dx.doi.org/10.1002/anie.201510376.

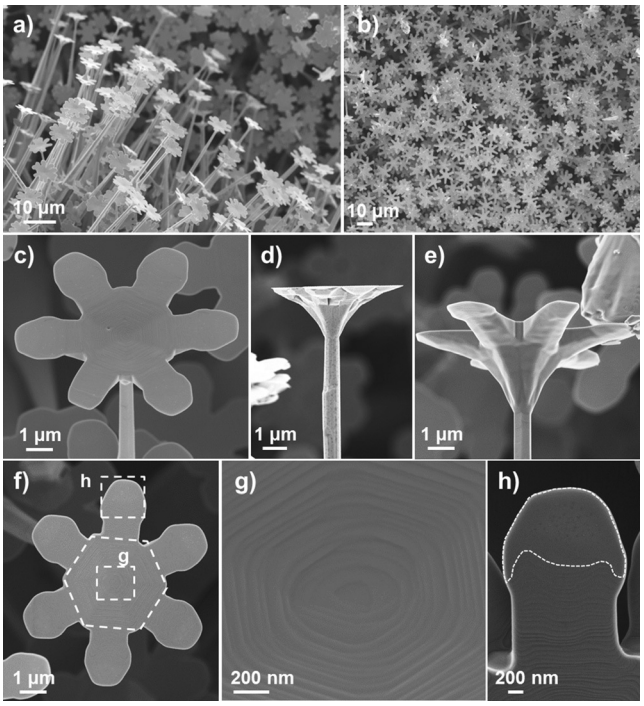

Figure 1. Morphologies of crown-caped NW structures. a) Large scale side view and b) top view of the crown-caped NW arrays. c) A tilted top view, d) a side view, and e) a tilted bottom view of an individual six-branched crown cap structure. f) A top view of the crown surface showing the hexagonal center pattern. g) Enlarged image on the crown center, showing the hexagonal concentric steps. h) Enlarged image on one branch, showing a large flat surface area around the tip of the branch and the steps became more regularly spaced near the center region.

and six branches, which expanded up to 7 μm wide. The side view in Figure 1 d shows that the crown had a basin-like shape, where the diameter gradually increased from ≈500 nm at the NW junction to ≈7 μm at the top. When observed from the bottom (Figure 1 e), the junction between the NW and crown showed a very smooth transition and no discontinuity could be identified.

The top view (Figure 1 f) reveals more details about the surface features of the crown. The crown center had a hexagonal outline, as marked by the white dashed line, and six branches grew out from the six edges of the hexagon. The enlarged view of the plate center (Figure 1 g) shows the surface was featured by concentric hexagonal circular steps. There was a flat surface at the innermost circle, and no screw dislocation spiral center could be identified. In contrast to our previous observations, the step height increased from the plate center to plate edge, forming a concave surface instead of the classic mount-shaped feature. A similar step structure could also be observed on the branch surface (Figure 1 h). At the very front branch tip region, a relatively wide flat surface area was commonly observed, which could be more than 1 μm wide. The initial steps exhibited larger step widths than the steps in the center region. The front of each step was not straight and does not represent any crystal facets. The flat area also covered a small area along the edge of the branches, as marked by dashed lines, indicating edge nucleation and growth was much more favorable than other positions on the plate. These morphological features suggested that new atomic layers would nucleate first at the edge, propagate inward, and slow down when approaching the previous step owing to the limited quantity of adatoms on the surface.

The crystal structure of the crown and junction region was characterized by transmission electron microscopy (TEM). A low-magnification bright-field TEM image (Figure 2 a) shows

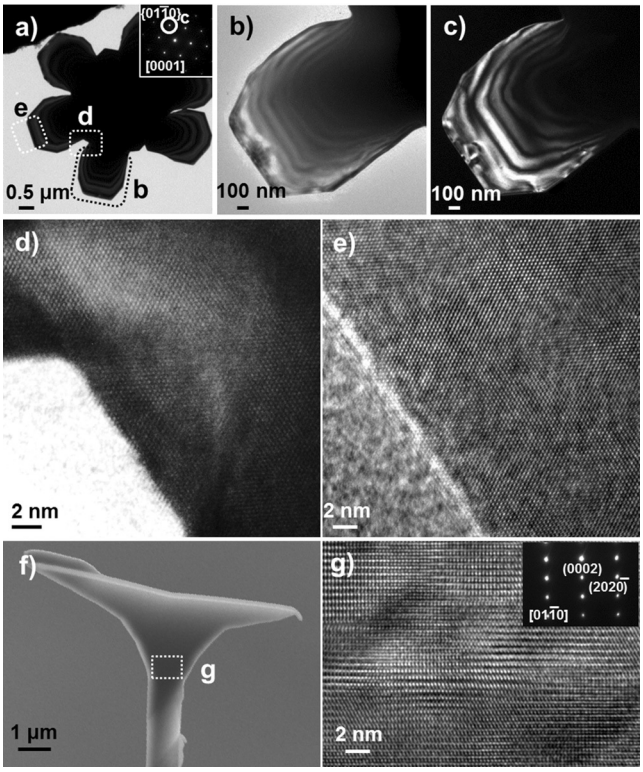

Figure 2. Crystal structure characterization on an individual crown. a) A low magnification TEM image showing the crown cap consists of six branches and a hexagonal core. Inset is the SAED along the [0001] zone axis. b) Bright field and c) dark field TEM images at crown branch showing the thickness increases from the branch tip to plate core, indicated by the thickness fringes. The dark field image was recorded using a {01$\bar{1}$0} reflected beam. d, e) High resolution TEM (HRTEM) images from the branch-core joint region (d), and branch edge (e). f) A cross-sectional slice of a crown-caped nanopillar prepared by focused ion beam along the axial direction. g) HRTEM image at the crown-NW joint region showing a perfect lattice without any dislocation, such as screw dislocation cores.

an entire crown that was removed from a NW tip, where the faceted core plate and branches could be clearly identified. The selected area electron diffraction (SAED; inset of Figure 2 a) revealed that the entire crown was a single crystal with the wurtzite crystal structure. Bright-field TEM images (Figure 2 b) and dark-field TEM images (Figure 2 c) were taken from one of the six branches along the [0001] zone axis. The thickness fringes can be clearly seen around the branch edge area, revealing thickening pattern from the branch tip towards the crown center. High-resolution TEM (HRTEM) images (Figure 2 d and e) revealed the good crystalline quality

at the connection area between the branch and the center plate, and at the branch edge, respectively. To observe the cross section, the nanostructure was cut into a slice along its axial direction using a focused ion beam (FIB) (Figure 2 f). HRTEM images were taken from the joint part between the crown and the NW. As shown in Figure 2 g, the lattice was continuous at the connection and no dislocation core could be observed. The SAED pattern in the inset of Figure 2 g also confirmed the single crystal feature of the entire hybrid structure.

Atomic force microscopy (AFM) was performed at the central plate area to analyze the surface steps, a very important feature toward understanding the growth mechanism. Figure 3 a shows an AFM topography image on the left

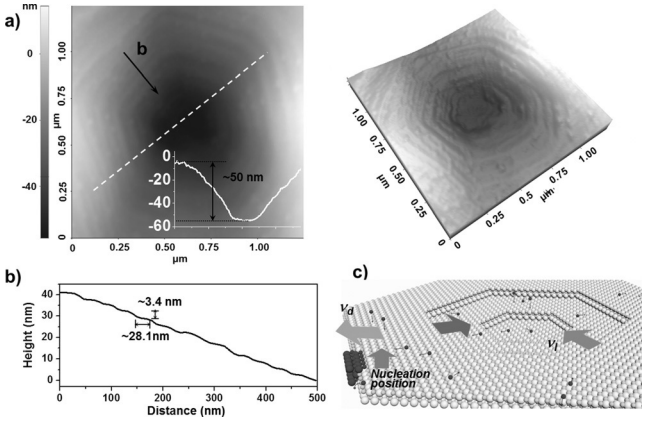

Figure 3. Step characterization and inverted wedding cake growth model. a) AFM topography image of the center area of the crown cap (left). Inset is a height profile along the dashed line, revealing the basin shape of the crown structure. The corresponding 3D AFM image of the same area is shown on the right. b) Height profile of the crown surface along the red arrow in (a), showing the step height is 3.4 nm and the width is 28.1 nm. c) Mechanism of the inverted wedding cake growth, where the nucleation was occurred along the plate edge. Blue arrows indicate the step propagation inwards. Red arrow indicates the plate expansion outwards through adatoms flipping over the plate edge.

and 3D surface construction on the right. From the topography image, many concentric circular steps could be observed. The height profile (inset of Figure 3 a) revealed that the center area had the lowest profile and the step heights increased around the edges. Such a concave structure could be more clearly observed from the 3D resembled image. It revealed a flat central base and concentric terraces with raising height, which are important features of the wedding cake growth mechanism. Since a regular wedding cake growth usually leads to a convex mount structure, this high-edge basin-like structure was an inversed morphology of a surface mount. Thus, this growth was regarded as an inverted wedding cake growth. From the AFM characterization, the step height and width were found to be fairly uniform with values of 3.4 nm and 28 nm, respectively (Figure 3 b). The step height was much larger than the lattice spacing of ZnO [0001], indicating the step bunching effect occurred during the step propagation.

Figure 3 c depicts the general growth process of the inverted wedding cake mechanism. In this model, the layer-by-layer growth was initiated at the plate edge instead of nucleating at the center as regular wedding cake growth. The newly formed atomic layers then propagated toward the plate center as adatoms adsorbed and diffused toward the nucleation sites, which thus formed a circular step along the plate edge. The expansion of the top surface is a result of the diffusion down of the adatoms by overcoming the ES barrier. Since the ES barrier prevents the adatoms from overcoming the crystal ledge, it helps increase the concentration of surface adatoms and thus facilitates the nucleation of new atomic layers. According to our previous results,[5c] as the supersaturation (σ) decreases, the chance for adatoms to overcome the ES barrier rises, while the concentration of surface adatoms drops. At a certain small σ, the top surface would become no longer a favorable place for nucleation of new atomic layers owing to the reduced adatom concentration. Instead, the adatom concentration rises at the crystal edge which becomes a new nucleation site. Therefore, new atomic layers start to form along the edge of the top surface while it becomes wider as the adatoms continuously attach to the edge. In typical mount morphology, the top layer has the largest flat area owing to the slower nucleation rate compared to the ledge expansion rate (nucleation-limited region). Similarly, in the inverted wedding cake growth, the top most layer, which is the surface along the edges of the branches, also exhibited the largest flat surface area (Figure 1 h). As the steps approaching the center area, the space between them became much smaller. This is consistent with the fact that the step growth slows down when it approaches the growth front of its previous one owing to the decrease of the effective adatom diffusion area, suggesting a mass-transport-limited growth region.

Such hybrid morphology could be received from a relatively broad σ range. Under a large deposition temperature range from 1470 K to 1600 K, all the NWs were crowned with a much wider basin-shaped structure containing six equivalent branches. However, the branches exhibited different morphologies owing to the slight variation of σ (Supporting Information, Figure S1). A possible reason may be that σ has slightly different influence on the ES barrier energy and/or the nucleation energy barrier on different top crystal side facets. Because it does not influence the general edge nucleation phenomenon, the branch morphology variation will not be further analyzed here.

To further understand how the inverted wedding cake growth is related to conventional wedding cake growth of NWs, a series of syntheses with different oxygen partial pressures were conducted. The oxygen partial pressures and the temperature zones would modify both the condensation and oxidation rates of zinc, and thus influence the growth kinetics. Representative morphologies are summarized in Figure 4 a and the corresponding large scale images are shown in the Supporting Information (Figure S2). In the highest temperature region, the nanostructures appeared in the form of NWs with a clear mount-shaped top surface. In the medium temperature zone, a hexagonal plate appeared at the top of each NW and a concave center started to develop. As the

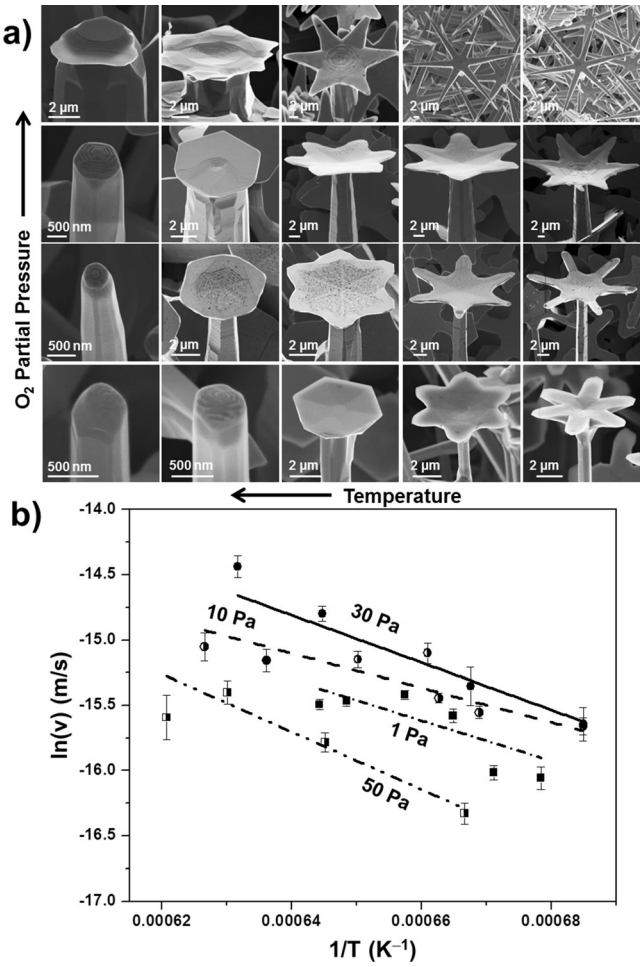

Figure 4. Morphology evolution with deposition temperature and O_2 partial pressure. a) SEM image map showing the evolution of crown-caped NW morphology influenced by different deposition temperatures and oxygen partial pressures. b) Relationship between the growth rate of crown plates/branches and temperature under different oxygen partial pressure, 1 Pa, 10 Pa, 30 Pa, and 50 Pa. The corresponding lines are fitted curves which give similar slopes, revealing the activation energy for overcoming the ES barrier. Each dot is the average value of ten sets of experimental data from the same temperature region and error bars show standard error.

temperature further reduced, the top plate clearly showed the basin shape and six equivalent branches evolved and elongated from the plate edge. The size of the plates also increased when lowering the deposition temperature. When applying different oxygen partial pressures, the same trend was observed. NW morphology was obtained at the lowest oxygen partial pressure. Increasing the oxygen partial pressure led the top morphology evolution from mount-shape hexagonal plates to basin-shaped branched structures.

The unique morphology switching phenomenon could be understood by the dynamic deposition condition change during the growth processes. At the beginning, the deposition temperature was relatively low, which keeps the equilibrium partial pressure (P_e) at a relatively low level. Since the precursor vapor concentration (P) remained at a relatively high level, σ at any deposition temperature (corresponding to the deposition position) was large (Supporting Information, Figure S3). This condition favored NW growth through the layer-by-layer wedding cake model along the [0001] direction. At this stage, the adatoms were confined at the top (0001) surface and diffusing down was significantly restricted by the ES barrier.[9] As the deposition temperature rises, P_e increased rapidly leading to a quick drop of σ. The reduction of σ was the most prominent at the highest deposition temperature region, leaving insufficient time for crown formation. Thus, NWs with a mount-shaped tip was obtained as the final product. Meanwhile, relatively small σ still remained at lower deposition temperature zones (Supporting Information, Figure S3c). Such a condition favored the diffusion down of the adatoms from the top surface by overcoming the ES barrier[10] and nucleated an additional layer circling around the tip of the NW broadening the top layer. As the diffusion down proceeded, the top surface became undersaturated for nucleating new atomic layers and the growth was completely initiated from the edge. Thus, the growth mode switched to the inverted wedding cake growth and the hexagonal crowns were formed. The growth could be terminated at this stage when P_e further increased to diminish σ at the medium deposition temperature zone. However, at the even lower deposition temperature region, σ could be favorable for lateral growth and larger crowns were obtained in that region. The appearance of six branches might be a result of oxygen adsorption that selectively restricted the growth on the flat edge area.[11] High oxygen partial pressure hinders the decomposition of ZnO precursor and thus lowers σ. Thus, the high oxygen partial pressure favors the growth of the crown featured morphologies and also promotes the formation of branched structure.

In general, the plate expansion is a kinetic process, which is determined by the diffusion down rate (α). The relationship between α and the ES barrier (E_{ES}) follows the equation:[10a]

$$\alpha = \exp(-\frac{E_{ES} - E_{sd}}{kT}) \quad (1)$$

where E_{sd} is the surface diffusion barrier, k is the Boltzmann constant, and T is temperature. Therefore, the deposition temperature-related plate morphology can be used to identify the ES barrier for ZnO nanostructure growth. From Equation (1), the growth rate of the suspended plate owing to adatom diffusion down to the edge (v_d) can be derived as a function of T (Supporting Information).

$$\ln v_d = \ln \frac{a^4}{\delta\sqrt{2\pi mk}} - \left(\frac{E_{ES} - E_{sd} + \Delta U}{k} + 9087.7\right)\frac{1}{T} \quad (2)$$

where a is the distance between adsorption sites, ΔU is the kinetic barrier for the incorporation of the building units into the half crystal, δ is average spacing of the kink sites, and m is the mass of zinc. v_d can be determined by comparing the suspended length and the corresponding height of plates, which represents the ratio between vertical growth rate and diffusion down rate. Through this method, v_d was identified from each temperature zone from samples grown under different oxygen partial pressures. The Arrhenius plots of $\ln v_d$

versus $1/T$ under the four selected oxygen partial pressures are shown in Figure 4b. The linear fits of the data exhibited very close slopes, from which the ES barrier E_{ES} was found to be 0.88 ± 0.33 eV. Compared to the reported values in other materials (0.52 eV for Au, 0.40 eV for Cu, and 0.12 eV for Al),[10b,12] the value we identified was much higher. This could be the reason that the diffusion down phenomenon was not commonly observed in oxide nanocrystals.

In conclusion, we have shown a unique hybrid nanostructure featured by branch-crowned NWs through high temperature non-isothermal VS deposition. An inverted wedding cake growth model was proposed to explain the formation of the nanostructures. The general formation mechanism was attributed to the largely raised adatom diffusion down rate due to lowering σ. Quantitative analysis found the ES barrier of ZnO was 0.88 ± 0.33 eV from a series of experiments with different oxygen partial pressures and different deposition temperatures. This research disclosed a nanostructure growth mechanism that sets a successful example of adopting traditional crystal growth mechanisms in understanding the formation of nanoscale morphologies. Given the fact that wedding cake growth has been discovered in many different material and crystal systems, we envision that the inverted wedding cake growth phenomenon might broadly exist in other crystal structures with appropriately controlled ES barriers, which will provide valuable knowledge for rational design and controlled synthesis of nanomaterials.

Acknowledgements

The authors thank financial support from Air Force Office of Scientific Research under Award FA9550-13-1-0168.

Keywords: 2D nanostructures · Ehrlich–Schwoebel barrier · oxides · supersaturation · wedding cake growth

How to cite: *Angew. Chem. Int. Ed.* **2016**, *55*, 2217–2221
Angew. Chem. **2016**, *128*, 2257–2261

[1] a) P. J. M. Smeets, K. R. Cho, R. G. E. Kempen, N. A. J. M. Sommerdijk, J. J. De Yoreo, *Nat. Mater.* **2015**, *14*, 394–399; b) R. W. Day, M. N. Mankin, R. Gao, Y.-S. No, S.-K. Kim, D. C. Bell, H.-G. Park, C. M. Lieber, *Nat. Nanotechnol.* **2015**, *10*, 345–352; c) S. Ye, Z. Chen, Y.-C. Ha, B. J. Wiley, *Nano Lett.* **2014**, *14*, 4671–4676.

[2] a) A. P. Alivisatos, *Science* **1996**, *271*, 933–937; b) D. Kim, Z. Shi, C. B. Simmons, D. R. Ward, J. R. Prance, T. S. Koh, J. K. Gamble, D. E. Savage, M. G. Lagally, M. Friesen, S. N. Coppersmith, M. A. Eriksson, *Nature* **2014**, *511*, 70–74; c) L. Qian, Y. Zheng, J. Xue, P. H. Holloway, *Nat. Photonics* **2011**, *5*, 543–548; d) S. A. McDonald, G. Konstantatos, S. G. Zhang, P. W. Cyr, E. J. D. Klem, L. Levina, E. H. Sargent, *Nat. Mater.* **2005**, *4*, 138–142.

[3] a) Y. Huang, X. F. Duan, Q. Q. Wei, C. M. Lieber, *Science* **2001**, *291*, 630–633; b) A. I. Boukai, Y. Bunimovich, J. Tahir-Kheli, J.-K. Yu, W. A. Goddard III, J. R. Heath, *Nature* **2008**, *451*, 168–171; c) M. Law, D. J. Sirbuly, J. C. Johnson, J. Goldberger, R. J. Saykally, P. D. Yang, *Science* **2004**, *305*, 1269–1273.

[4] a) K. S. Novoselov, A. K. Geim, S. V. Morozov, D. Jiang, M. I. Katsnelson, I. V. Grigorieva, S. V. Dubonos, A. A. Firsov, *Nature* **2005**, *438*, 197–200; b) Y. B. Zhang, Y. W. Tan, H. L. Stormer, P. Kim, *Nature* **2005**, *438*, 201–204; c) H. Yang, D. Zhao, S. Chuwongin, J.-H. Seo, W. Yang, Y. Shuai, J. Berggren, M. Hammar, Z. Ma, W. Zhou, *Nat. Photonics* **2012**, *6*, 615–620.

[5] a) R. S. Wagner, W. C. Ellis, *Appl. Phys. Lett.* **1964**, *4*, 89–90; b) G. A. Bootsma, H. J. Gassen, *J. Cryst. Growth* **1971**, *10*, 223–234; c) X. Yin, J. Shi, X. Niu, H. Huang, X. Wang, *Nano Lett.* **2015**, *15*, 7766–7772.

[6] a) C. Y. Wen, M. C. Reuter, J. Tersoff, E. A. Stach, F. M. Ross, *Nano Lett.* **2010**, *10*, 514–519; b) S. Hofmann, R. Sharma, C. T. Wirth, F. Cervantes-Sodi, C. Ducati, T. Kasama, R. E. Dunin-Borkowski, J. Drucker, P. Bennett, J. Robertson, *Nat. Mater.* **2008**, *7*, 372–375; c) H. Cui, Y. Y. Lu, G. W. Yang, Y. M. Chen, C. X. Wang, *Nano Lett.* **2015**, *15*, 3640–3645.

[7] a) Y. Liu, M. Liu, *Adv. Funct. Mater.* **2005**, *15*, 57–62; b) Q. Ji, Y. Zhang, T. Gao, Y. Zhang, D. Ma, M. Liu, Y. Chen, X. Qiao, P.-H. Tan, M. Kan, J. Feng, Q. Sun, Z. Liu, *Nano Lett.* **2013**, *13*, 3870–3877.

[8] a) R. L. Penn, J. F. Banfield, *Science* **1998**, *281*, 969–971; b) W. K. Burton, N. Cabrera, C. Frank, *Philos. Trans. R. Soc. London Ser. A* **1951**, *243*, 299–358.

[9] a) G. Ehrlich, F. G. Hudda, *J. Chem. Phys.* **1966**, *44*, 1039–1049; b) R. L. Schwoebel, E. J. Shipsey, *J. Appl. Phys.* **1966**, *37*, 3682–3686.

[10] a) J. Tersoff, A. W. D. Vandergon, R. M. Tromp, *Phys. Rev. Lett.* **1994**, *72*, 266–269; b) X. Niu, S. P. Stagon, H. Huang, J. K. Baldwin, A. Misra, *Phys. Rev. Lett.* **2013**, *110*, 136102.

[11] a) K. Subannajui, N. Ramgir, R. Grimm, R. Michiels, Y. Yang, S. Mueller, M. Zacharias, *Cryst. Growth Des.* **2010**, *10*, 1585–1589; b) V. Craciun, S. Amirhaghi, D. Craciun, J. Elders, J. G. E. Gardeniers, I. W. Boyd, *Appl. Surf. Sci.* **1995**, *86*, 99–106.

[12] a) S. K. Xiang, H. Huang, *Appl. Phys. Lett.* **2008**, *92*, 101923; b) S. Lee, H. Huang, *Nanoscale Res. Lett.* **2011**, *6*, 559.

Received: November 8, 2015
Revised: December 6, 2015
Published online: January 6, 2016

